

Measurement of the electric field distribution in streamer discharges

Yihao Guo¹, Anne Limburg¹, Jesse Laarman¹, Jannis Teunissen², Sander Nijdam^{1*}

¹*Department of Applied Physics and Science Education,*

Eindhoven University of Technology, 5600 MB Eindhoven, The Netherlands

²*Centrum Wiskunde & Informatica (CWI), 1090 GB Amsterdam, The Netherlands*

(Dated: October 14, 2024)

Using electric field induced second harmonic generation (E-FISH), we performed direction-resolved absolute electric field measurements on single-channel streamer discharges in 70 mbar (7 kPa) air with 0.2 mm and 2 ns resolutions. In order to obtain the absolute (local) electric field, we developed a deconvolution method taking into account the phase variations of E-FISH. The acquired field distribution shows good agreement with the simulation results under the same conditions, in direction, magnitude and in shape. This is the first time that E-FISH is applied to streamers of this size (>0.5 cm radius), crossing a large gap. Achieving these high resolution electric field measurements benefits further understanding of streamer discharges and enables future use of E-FISH on cylindrically symmetric (transient) electric field distributions.

Streamer discharges are fast propagating ionization fronts that appear as the precursor to lightning leaders and as sprites in nature [1]. The electric field is the driving force behind streamers and determines their energy transfer and chemical activity [2]. There are various studies focusing on electric field measurement of discharges using different diagnostics, including electric-field-induced coherent anti-Stokes Raman scattering (E-CARS) [3] and Stark spectroscopy [4]; while methods for measuring the electric field in streamers, which are highly transient, are limited, and if present, have very low temporal and spatial resolution. Most recently, Dicks *et al.* [5] determined the electric field of single-channel streamers in pure nitrogen and synthetic air at pressures of 33 mbar by using optical emission spectroscopy (OES). However, this method has the disadvantages that it depends on light emission, cannot measure the field direction and has a rather low spatial and temporal resolution. The lack of suitable methods hinders further understanding of streamers and other transient discharges driven by the electric field.

To tackle these problems, a new technique called electric field induced second harmonic generation (E-FISH) has been introduced to the plasma community to measure the electric field of various kinds of plasmas [6, 7]. In this method, a high power laser beam non-linearly interacts with an electric field in a gas, generating second harmonics. The intensity of these second harmonics scales directly with the square of the electric field strength, and the polarization direction aligns with the field orientation. Initially, this method was considered easy to implement and the measured signals straightforward to interpret. However, it has been shown that the measured signals are strongly related to the laser beam profile, and depend heavily on the electric field profile and not just its integrated value due to phase variations along the laser beam [8]. A solution has been proposed

in [9], but uniformity of the electric field in one of the directions perpendicular to the laser beam is assumed, which is not a valid assumption for streamers.

In this Letter, for the first time, we report detailed direction-resolved measurements of the electric field distribution in single-channel streamers in air by using E-FISH. The electric field is restored from the E-FISH signals by applying a deconvolution method including all phase variations, where cylindrical symmetry is assumed. Also, light emission from the discharge is captured. Next to this, simulations on the electric field and the emission spectrum of the second positive system (SPS) of N_2 are obtained using a 2D axisymmetric drift-diffusion-reaction fluid model [10] of the streamers under the same conditions. Li *et al.* [10] have shown that this model is very reliable in simulating streamers in air; its calculated streamers closely match in velocities and diameters with experimental results.

The experimental results show a tremendous improvement in resolution compared to previous work. Thus far, such detailed electric field distributions of transient plasmas could only be obtained through simulations. Moreover, we reveal the electric field in areas with little to no light emission, which contains the most valuable information for streamer discharges. The magnitude, shape and direction of the field and its position relative to the light emission are in agreement with the simulations. This enables further understanding of streamers and empowers future use of E-FISH.

A schematic of the experimental setup is shown in Fig. 1. In short, a 100 mJ Nd:YAG laser (EKSPLA SL234-10-G-SH) beam with a pulse width of 120 ps at 1064 nm is focused into the discharge area by an $f = 500$ mm lens. The beam waist and Rayleigh length z_R are measured to be 0.13 mm and 12 mm, respectively, by using the knife edge method [11]. Two longpass filters remove any second harmonic light generated by the laser itself and by interaction between the laser beam and the upstream optics. Second harmonic light is generated when the laser interacts with the electric field in the streamers that are produced inside a vessel. The

* s.nijdam@tue.nl

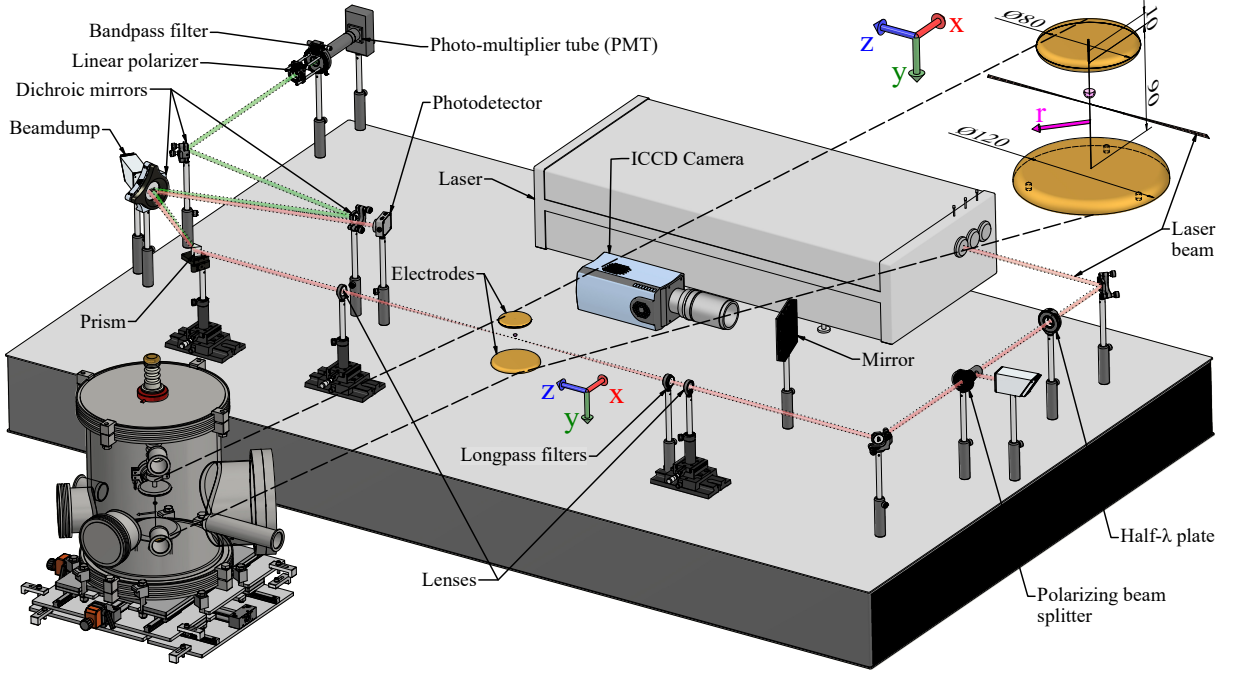


Figure 1. A render of the E-FISH setup. The vacuum vessel is excluded from the main image for clarity and is instead shown on the bottom left. We use a coordinate system in which the streamer propagates in the y direction, the laser beam is along the z direction, and the radial coordinate is given by $r = \sqrt{x^2 + z^2}$. The detailed geometry of the electrodes including streamer, r -direction definition, and the laser beam (dimensions in mm) is shown on the top right.

fundamental and second harmonic beams are collimated again by another $f = 500$ mm lens. These two collinear beams are then fully separated by using a prism and three dichroic mirrors. The fundamental beam intensity is measured by a photodetector (Thorlabs DET36A/M). The second harmonic beam is directed to a photomultiplier (PMT, Hamamatsu H6779-04), with a bandpass filter attached in front of it to filter out any stray light. To increase the signal-to-noise ratio, the laser beam is polarized parallel to the to-be-measured electric field direction by using a half-wave plate and a polarizer, because the second harmonic generation process has a higher efficiency under this configuration [7]. A polarizer is positioned in front of the PMT to measure the vector components of the electric field.

To generate streamers, we use the setup that has been described in [5]. The high voltage pulses are generated by a pulsed power circuit (Belhke HTS) with an amplitude of 9.5 kV, a rise time of about 50 ns, a voltage jitter of ~ 1 ns, and a duration of 400 ns at a repetition rate of 60 Hz. The electrodes are protrusion-to-plane electrodes, where the high voltage electrode contains a 10 mm protruding pin in the center (1 mm diameter, 60° tip angle, and 50 μ m tip radius). The pin-to-plate gap is 90 mm. The laser beam is at the height of 5.3 cm from the grounded bottom plate electrode. During the experiment, the vessel is continuously flushed with dry air with a flow rate of 2 L/min and the pressure is fixed at 70 mbar (7 kPa). The pulse repetition rate, the dedicated electrode geometry,

and the reduced pressure ensure the high repetitiveness in both time and space of the single positive streamers, and thus the quality of the E-FISH signals.

The moment the laser interacts with the streamer electric field, the discharge image is captured by an ICCD camera (Andor DH334T) with a gating time of 2 ns. From these images, only a horizontal strip at the height of the laser beam is used. Under the above mentioned conditions, the streamer propagation velocity is measured to be 3.5×10^5 m/s. The laser, the high voltage pulses, and the gating of the ICCD camera are synchronized by a digital delay generator.

In order to obtain the electric field at different positions in the discharge, the entire vessel is fixed on a translation stage such that it can move over the horizontal axis (coordinate x) perpendicular to the laser beam direction (coordinate z). The second dimension is acquired by varying the delay between the high voltage pulse (and consequently streamer inception) and the laser trigger. This allows us to generate an image with time as one dimension and the horizontal cross-section of the streamer in the second dimension both for optical emission and electric field strength. Because the single-channel streamers under investigation are roughly constant in shape and velocity when traversing the center of the electrode gap [10], the time axis is very similar to the streamer propagation direction axis (coordinate y). For a single measurement of one field direction, a time range of -80 to 120 ns with a step size of 2 ns and a spatial range of -15 to 15 mm

with a step size of 0.2 mm is used, where $t = 0$ is defined as the moment when the electric field in the y -direction peaks, and $x = 0$ the middle of the streamer in the x -direction. For every delay and position, 40 laser shots are recorded, resulting in one measurement consisting of more than 400,000 laser shots (the grid size is coarser for the lower field region). A full measurement, for both directions of the electric field, takes about 15 hours.

The signal we measure is $s(x, t) = \sqrt{I_{2\omega}/I_\omega^2}$, where $I_{2\omega}$ and I_ω represent the intensity of the second harmonic and fundamental beams, respectively. This signal is the result of a line-of-sight integration along the laser propagating direction [8, 12]:

$$s(x, t) = C_{\text{cal}} \left| \int_{-L}^L \frac{e^{-i\Delta k z}}{1 + i \frac{z}{z_R}} E_{\text{ext}}(x, z, t) dz \right|, \quad (1)$$

where C_{cal} is a calibration constant; $2L$ is the interaction length of the laser beam and the electric field; Δk is the wavevector mismatch between the fundamental and second harmonic wavelengths, z_R is the Rayleigh length of the focused beam, and E_{ext} the external, to-be-measured electric field of which the x - and y -component can be measured. Δk is 3.45 m^{-1} for 70 mbar air with a 1064 nm input beam [13]. The complex denominator, $1 + i \frac{z}{z_R}$, introduces an extra phase shift $\tan^{-1} \frac{z}{z_R}$ called Gouy phase, which originates from the focused Gaussian beam shape. For an axisymmetric streamer, the electric field in the y -direction E_y will also be axisymmetric, such that $E_{\text{ext}}(x, z, t) = E_y(r, t)$ where $r = \sqrt{x^2 + z^2}$. We can also make use of the axisymmetry when measuring the field in the x -direction E_x , by expressing it as $E_x = \sin(\theta)E_r$, where E_r is the axisymmetric radial component and $\sin(\theta) = x/r$. In this case, we thus have $E_{\text{ext}}(x, z, t) = x/r E_r(r, t)$.

We cannot use a standard inverse Abel transform to solve equation (1). Instead, we approximate the integral by a weighted sum over samples $E_y(r_i)$ or $E_r(r_i)$, at a given set of radial coordinates. Given a set of measurements $s(x_j)$, we can then solve an approximately linear system to obtain $E_x(r_i)$ or $E_y(r_i)$. We include a small regularization parameter in this procedure to make the inversion unique and robust to noise in the measurements. A detailed description of the inversion procedure is given in the supplementary material [14]. Similarly, the optical emission is Abel-inverted.

To obtain the absolute field strength, a calibration measurement on a known field distribution is performed. We designed rod-to-rod and rod-to-cylinder electrodes for the calibration of E_y and E_x , respectively, which generate an electric field with a similar shape as the streamer. First, the electrostatic field of these configurations is simulated in COMSOL Multiphysics. Then the field is forward-transformed by using the inverse of the algorithm described above to obtain the “calculated E-FISH signals”. The ratio between the calculated signals and the measured signals leads to the calibration constant C_{cal} .

Figure 2 shows the amplitudes of the E-FISH signals for E_y and E_x of a single-channel streamer in 70 mbar air with an applied voltage of 9.5 kV. It is worth noting that the distribution of the E_x signals can become asymmetric around $r = 0$ due to interference between the E-FISH signal and the background signal. We discuss this issue, its implications on other E-FISH results and corresponding solutions in detail in the supplementary material [14].

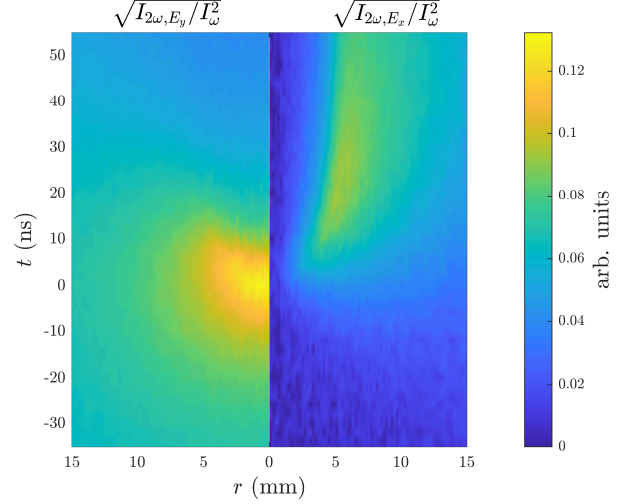


Figure 2. Measured E-FISH signals for E_y (left) and E_x (right) of a streamer in 70 mbar air with an applied voltage of 9.5 kV. $t = 0$ is defined as the time when E_y peaks.

By using the deconvolution method described, and multiplying with calibration constant C_{cal} , the absolute values of both the r and y components of the electric field can be restored from the signals. The magnitude of the electric field is calculated as $|E| = \sqrt{E_r^2 + E_y^2}$. Figure 3 shows the comparison of local light emission intensity and electric field distribution between experiment and simulation results. $|E|/N$ is the absolute reduced electric field in Townsend (Td, E/N in units $10^{-21} \text{ V}\cdot\text{m}^2$), where N is the gas number density. Here, N equals $1.88 \cdot 10^{24} \text{ m}^{-3}$ at 70 mbar when assuming room temperature. In the simulation, the conditions in [10] are adapted to fit the voltage and pressure used in this experiment. The emitted light is estimated by the $\text{N}_2(\text{C}^3\Pi_u)$ density because the SPS transition is responsible for most of the optical emission under our discharge conditions [15]. Note that the simulation only treats one voltage pulse, therefore the heating effect of repetitive pulses is not taken into account. In the experiments the gas temperature will likely be elevated above room temperature [16, 17], but its exact value cannot be determined in this setup.

Qualitatively, the experimental and simulation results exhibit very high visual similarity. In both cases the space charge layer with the crescent shape of the streamer head is clearly visible. The electric field is most intense around the head of streamers and mostly pointing downwards. Inside the streamer channel, the electric

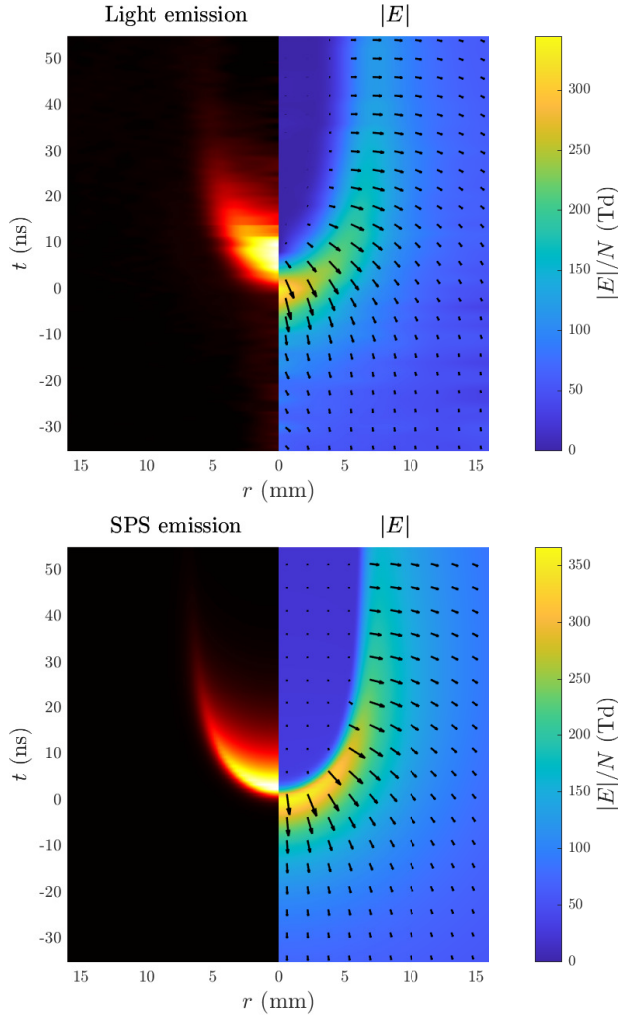


Figure 3. Experimental (top) and simulation (bottom) results of local normalized light emission intensity and reduced electric field distribution.

field almost vanishes, as the highly conductive streamer channel shields the electric field very efficiently. Furthermore, the light emission always lags behind the electric field [18, 19]. Thus, light emission based methods to measure the electric field can only determine the field in the area behind the peak electric field, while E-FISH can resolve the field distribution completely. In the simulation, the light emission profile shows a sharp front, while in the experiment it is smeared out more and shows some internal structure. The smearing is partly due to the camera integration time and streamer jitter, while the internal structure is attributed to oscillating ripples in the voltage waveform that change the velocity of the streamers.

Quantitatively, the streamers in both cases have similar size and very close field magnitude. The electrodynamic diameter measured by the electric field is defined as the radial position at which E_r reaches a maximum. In experiment and simulation these are 7.4 mm and 7.8 mm respectively for $t = 50$ ns, which agrees very well.

Figure 4 shows a comparison of the axial field evolution and light emission, and of the radial field and light emission at 50 ns between experiment and simulation. In

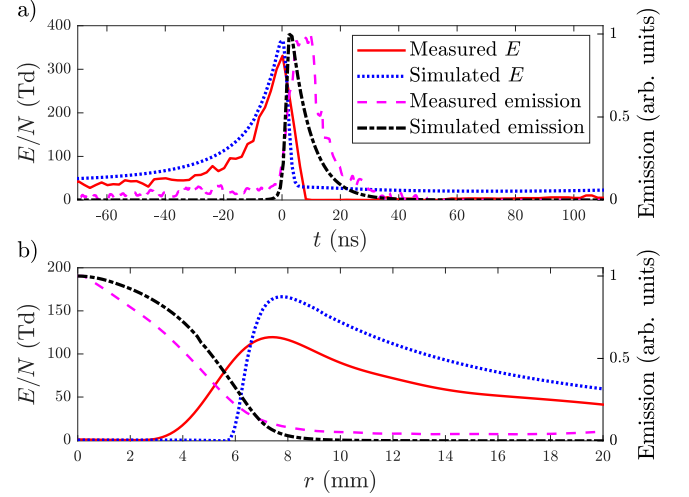


Figure 4. A comparison of a) the axial field (E_y) and light emission and b) the radial field (E_r) and light emission between E-FISH experiment and simulation. The radial field was determined at 50 ns while the radial light emission was integrated over the entire time domain and normalized to its maximum.

figure 4(a), it is shown that the simulated and measured electric field stay roughly constant at the background field level and rise rapidly at around $t = -20$ ns when the streamer head is approaching the probing laser. The maximum electric field peaks at 364 Td and 320 Td for simulation and experiment, respectively. These values correspond to $6.4 \cdot 10^5$ V/m and $5.6 \cdot 10^5$ V/m respectively. The difference between experiment and simulation is likely caused by the temporal resolution of the experiment being limited by the streamer jitter and by a slightly elevated gas temperature in the experiments.

Subsequently, the axial field drops drastically within 5 ns and remains at almost zero, as the streamer leaves behind a conducting channel after the streamer head crosses. The peak value is higher than the breakdown threshold in air (~ 120 Td) and is lower than the field determined by OES in [5] with a peak field of 540 Td in 33 mbar air and in [19] around 500 Td at atmospheric pressure. Mrkvičková *et al.* [20] compared the electric field in an atmospheric pressure Townsend discharge in nitrogen determined by E-FISH and OES, and found that the OES method gives systematically higher values. They attributed this to the omission of additional population processes of $N_2^+(B^2\Sigma_u^+)$. In figure 4(b), the radial field profiles have similar shapes, except that the measured field has a smoother edge and lower peak value. This is probably due to the lower field intensity of the calibration measurement as well as a larger background signal of E_x , which results in a lower sensitivity. Outside the streamer channel, the radial fields in both cases

decay with approximately the same speed.

In conclusion, we have used E-FISH to determine for the first time an experimentally obtained detailed direction-resolved spatiotemporal distribution of the electric field in a single-channel streamer. Moreover, the electric field in areas with little to no light emission is revealed. The measurement was performed in 70 mbar air with resolutions of 0.2 mm and 2 ns. Simultaneously, the optical emission was tracked with a resolution of 2 ns. We developed a deconvolution method for E-FISH including the effect of phase variations and designed dedicated calibration experiments for cylindrically symmetrical fields to restore the absolute electric field distribution from E-FISH signals. Simulations on the electric field and SPS emission of the same streamer were obtained using a 2D axisymmetric drift-diffusion-reaction fluid model. We compared the experimental and simulation results and they show great agreement both qualitatively and quantitatively. The maximum electric field peaks at 364 Td and 320 Td for simulation and experiment, respectively. This enables us to further verify and validate the simulation models and have a comprehensive understanding of

streamer discharges in nearly all gas mixtures, both on the development and on the chemical processes inside.

It must be noted that for our discharge geometry and laser set-up, the difference in outcome between our full processing method and a more standard Abel inversion, for E_y is below 20%. However, the standard Abel inversion is more sensitive to noise from the outer regions and therefore requires more smoothing. For E_r , a standard Abel inversion is insufficient, as it cannot translate the E_x vector into E_r .

The developed method for analysing E-FISH measurements can be applied on highly repetitive plasmas/electric fields as a scan of the electric field is required. However, cylindrical symmetry is needed.

Future efforts should be directed to adjusting the analysis and corresponding methods to make E-FISH suitable for asymmetric fields. This will allow for high resolution direct electric field measurements of transient/fast moving electric fields in (ionized) gases, which is currently impossible.

Y G was supported by the China Scholarship Council (CSC) Grant No. 202006280041.

-
- [1] S. Nijdam, J. Teunissen, and U. Ebert, *Plasma Sources Science and Technology* **29**, 103001 (2020).
 - [2] A. K. Patnaik, I. Adamovich, J. R. Gord, and S. Roy, *Plasma Sources Science and Technology* **26**, 103001 (2017).
 - [3] M. van der Schans, P. Böhm, J. Teunissen, S. Nijdam, W. IJzerman, and U. Czarnetzki, *Plasma Sources Science and Technology* **26**, 115006 (2017).
 - [4] N. Cvetanović, M. M. Martinović, B. M. Obradović, and M. M. Kuraica, *Journal of Physics D: Applied Physics* **48**, 205201 (2015).
 - [5] S. Dijcks, L. Kusýn, J. Janssen, P. Bílek, S. Nijdam, and T. Hoder, *Frontiers in Physics* **11**, 10.3389/fphy.2023.1120284 (2023).
 - [6] A. Dogariu, B. M. Goldberg, S. O'Byrne, and R. B. Miles, *Physical Review Applied* **7**, 024024 (2017).
 - [7] T. L. Chng, M. Naphade, B. M. Goldberg, I. V. Adamovich, and S. M. Starikovskaia, *Optics Letters* **45**, 1942 (2020).
 - [8] T. L. Chng, S. M. Starikovskaia, and M.-C. Schanne-Klein, *Plasma Sources Science and Technology* **29**, 125002 (2020).
 - [9] S. Nakamura, M. Sato, T. Fujii, A. Kumada, and Y. Oishi, *Physical Review A* **104**, 053511 (2021).
 - [10] X. Li, S. Dijcks, S. Nijdam, A. Sun, U. Ebert, and J. Teunissen, *Plasma Sources Science and Technology* **30**, 095002 (2021).
 - [11] J. M. Khosrofi and B. A. Garetz, *Applied Optics* **22**, 3406 (1983).
 - [12] R. W. Boyd, *Nonlinear optics*, fourth edition ed. (Elsevier, AP Academic Press, London, 2020).
 - [13] A. Börzsönyi, Z. Heiner, M. P. Kalashnikov, A. P. Kovács, and K. Osvay, *Applied Optics* **47**, 4856 (2008).
 - [14] See Supplementary Material at [URL will be inserted by publisher] for details on the inversion procedure, calibration method, and interference issue, which includes Refs. [21, 22].
 - [15] S. V. Pancheshnyi, S. V. Sobakin, S. M. Starikovskaya, and A. Y. Starikovskii, *Plasma Physics Reports* **26**, 1054 (2000).
 - [16] S. Adams, J. Miles, T. Ombrello, R. Brayfield, and J. Lefkowitz, *Journal of Physics D: Applied Physics* **52**, 355203 (2019).
 - [17] D. Z. Pai, D. A. Lacoste, and C. O. Laux, *Journal of Applied Physics* **107**, 10.1063/1.3309758 (2010).
 - [18] E. Wagenaar, M. D. Bowden, and G. M. W. Kroesen, *Physical Review Letters* **98**, 075002 (2007).
 - [19] T. Hoder, Z. Bonaventura, A. Bourdon, and M. Šimek, *Journal of Applied Physics* **117**, 10.1063/1.4913215 (2015).
 - [20] M. Mrkvičková, L. Kuthanová, P. Bílek, A. Obrušník, Z. Navrátil, P. Dvořák, I. Adamovich, M. Šimek, and T. Hoder, *Plasma Sources Science and Technology* **32**, 065009 (2023).
 - [21] S. Raskar, K. Orr, I. V. Adamovich, T. L. Chng, and S. M. Starikovskaia, *Plasma Sources Science and Technology* **31**, 085002 (2022).
 - [22] S. Nakamura, M. Sato, T. Fujii, and A. Kumada, *Plasma Sources Science and Technology* **31**, 115020 (2022).

Supplementary material: Measurement of the electric field distribution in streamer discharges

Yihao Guo¹, Anne Limburg¹, Jesse Laarman¹, Jannis Teunissen² and Sander Nijdam¹

¹*Department of Applied Physics and Science Education, Eindhoven University of Technology, 5600 MB Eindhoven, The Netherlands*

²*Centrum Wiskunde & Informatica (CWI), 1090 GB Amsterdam, The Netherlands*

October 14, 2024

1 Signal inversion

As explained in the main text, we measure a signal $s(x, t)$ that results from either the longitudinal field E_y of an axisymmetric streamer or from its the radial field E_r . These cases correspond to the following integrals

$$s_y(x, t) = C_{\text{cal}} \left| \int_{-L}^L g(z) E_y(r, t) dz \right|, \quad (1)$$

$$s_r(x, t) = C_{\text{cal}} \left| \int_{-L}^L g(z) x/r E_r(r, t) dz \right|, \quad (2)$$

where $r = \sqrt{x^2 + z^2}$ and

$$g(z) = \frac{e^{-i\Delta k z}}{1 + i \frac{z}{z_R}}. \quad (3)$$

The meaning and values of Δk and z_R are discussed in the main text. Below, we will for brevity refer to $E_y(r, t)$ or $E_r(r, t)$ simply as $f(r)$. The dependence on t is left out as the inversion is performed for every t (line-by-line). The goal is to approximate $f(r_i)$ at given locations r_i ($i = 1, \dots, N$) from a set of samples $s(x_j)$ ($j = 1, \dots, M$), which is an inverse problem. If we have samples $\mathbf{f} = (f_1, f_2, \dots, f_N)$, then we can approximate the integral for a given x by weighted sum

$$s(x_j) \approx \left| \sum_{i=1}^N w_i f(r_i) \right|, \quad (4)$$

where the weights w_i still have to be determined, and where the factor C_{cal} has been left out for brevity. When we consider multiple x -positions simultaneously, we can express these sums as an approximately linear system of the form

$$|\mathbf{W}\mathbf{f}| = \mathbf{s}, \quad (5)$$

where \mathbf{f} and \mathbf{s} are real vectors, \mathbf{W} is a complex matrix, and the norm operator $||$ is applied element wise. Note that for any solution \mathbf{f} , $-\mathbf{f}$ is also a solution. We can solve such a system in the least-squares sense by minimizing the expression

$$|(|\mathbf{W}\mathbf{f}| - \mathbf{s})|. \quad (6)$$

In practice, it is typically necessary to include some regularization, to ensure that a unique solution exists and that the solution is not too sensitive to noise in the measurements. We include such regularization by minimizing the following expression

$$|(|\mathbf{W}\mathbf{f}| - \mathbf{s})| + c |\mathbf{f}''|, \quad (7)$$

where \mathbf{f}'' is an approximation of the second derivative of \mathbf{f} , given by $f_i'' = (f_{i-1} - 2f_i + f_{i+1})/(\Delta r)^2$, with Δr being the spacing between sampling points. For the inversions shown in the paper, we used $c = 3 \times 10^{-2} (\Delta r)^2$.

1.1 Obtaining the weight matrix

Below, we explain how we obtain the weight matrix \mathbf{W} in equation (5). The first step is to convert the line integrals into integrals over the radial coordinate r , as is also done in a standard Abel transform. Suppose we want to evaluate the following integral:

$$s(x) = \int_{-\infty}^{\infty} f(\sqrt{x^2 + z^2})g(z)dz, \quad (8)$$

where $r = \sqrt{x^2 + z^2}$, as above. We can change the integration variable to r , noting that

$$z = \pm \sqrt{r^2 - x^2}, \quad dz = \pm \frac{rdr}{\sqrt{r^2 - x^2}}. \quad (9)$$

Now split the integral in two parts

$$s(x) = \int_{-\infty}^0 f(\sqrt{x^2 + z^2})g(z)dz + \int_0^{\infty} f(\sqrt{x^2 + z^2})g(z)dz, \quad (10)$$

and then change variable in both parts, using the appropriate signs from equation (9):

$$s(x) = \int_{\infty}^{|x|} f(r)g(-\sqrt{r^2 - x^2})\frac{-r}{\sqrt{r^2 - x^2}}dr + \int_{|x|}^{\infty} f(r)g(\sqrt{r^2 - x^2})\frac{r}{\sqrt{r^2 - x^2}}dr. \quad (11)$$

This can be simplified to

$$s(x) = \int_{|x|}^{\infty} f(r) \left[g(\sqrt{r^2 - x^2}) + g(-\sqrt{r^2 - x^2}) \right] \frac{r}{\sqrt{r^2 - x^2}} dr. \quad (12)$$

To numerically evaluate equation (12), we for simplicity assume that the $\mathbf{f} = (f_1, f_2, \dots, f_N)$ are equally spaced, so that $r_{i+1} - r_i = \Delta r$. We furthermore assume that $f(r)$ and $g(z)$ do not vary strongly in each interval from $r_i - 0.5\Delta r$ to $r_i + 0.5\Delta r$. On the other hand, the factor $\frac{r}{\sqrt{r^2 - x^2}}$ will vary significantly (and diverge) for $r \rightarrow |x|$. Since

$$\int \frac{r}{\sqrt{r^2 - x^2}} dr = \sqrt{r^2 - x^2} + C, \quad (13)$$

we can handle this by analytically integrating this factor

$$\int_{r_i - 0.5\Delta r}^{r_i + 0.5\Delta r} \frac{r}{\sqrt{r^2 - x^2}} dr = \sqrt{(r_i + 0.5\Delta r)^2 - x^2} - \sqrt{(r_i - 0.5\Delta r)^2 - x^2}, \quad (14)$$

and then changing the integral to a sum:

$$s(x) \approx \sum_{i=1}^N f(r_i) \left[g(\sqrt{r_i^2 - x^2}) + g(-\sqrt{r_i^2 - x^2}) \right] \left(\sqrt{(r_i + 0.5\Delta r)^2 - x^2} - \sqrt{(r_i - 0.5\Delta r)^2 - x^2} \right). \quad (15)$$

Since the integral in equation (12) starts from $r = |x|$, only terms in the sum for which $r^2 - x^2 > 0$ should contribute. This can be achieved by replacing all terms of the form $r^2 - x^2$ by zero when they are negative.

If we consider equation (2) for E_r , there will be an extra factor $\sin(\theta) = x/r$ in equation (12), so that

$$s(x) = \int_{|x|}^{\infty} f(r) \left[g(\sqrt{r^2 - x^2}) + g(-\sqrt{r^2 - x^2}) \right] \frac{x}{\sqrt{r^2 - x^2}} dr. \quad (16)$$

The weight function for each sample f_i can again be integrated analytically:

$$\int \frac{x}{\sqrt{r^2 - x^2}} dr = x \log \left(2\sqrt{r^2 - x^2} + 2r \right) + C. \quad (17)$$

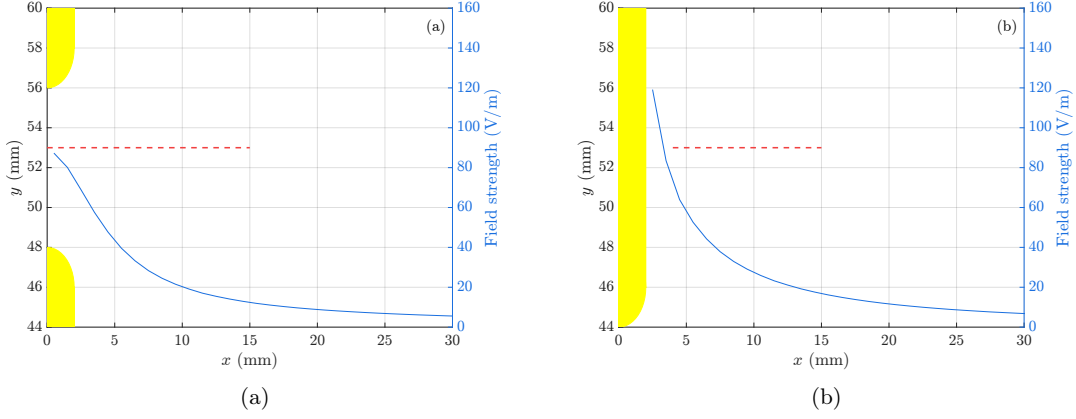


Figure 1: Calculated fields of (a) rod-to-rod electrodes for E_y and (b) rod-to-cylinder electrodes for E_x , respectively. The applied voltage for both configurations is 1 V. The shapes colored in yellow show the electrode geometry. The dotted red line indicates the height and the scan range of the laser.

This results in a sum

$$s(x) \approx \sum_{i=1}^N f(r_i) \left[g(\sqrt{r_i^2 - x^2}) + g(-\sqrt{r_i^2 - x^2}) \right] x \log \left(\frac{\sqrt{r_b^2 - x^2} + r_b}{\sqrt{r_a^2 - x^2} + r_a} \right), \quad (18)$$

where $r_a = r_i - 0.5\Delta r$ and $r_b = r_i + 0.5\Delta r$. Note that we used $\log(b) - \log(a) = \log(b/a)$. Again, the integral in equation (16) starts from $r = |x|$, so the sum should only contain corresponding contributions. This means that $\sqrt{r_a^2 - x^2} + r_a \geq |x|$ and similarly for r_b , so that these terms can be replaced by $\max(\sqrt{r_a^2 - x^2} + r_a, |x|)$. Since $\lim_{x \rightarrow 0} x \log(x) = 0$, the case $x = 0$ should give a zero contribution.

The right-hand sides of equations (15) and (18) contain the weights w_i for each of the $f(r_i)$. Computing these weights for different sampling locations x_j (i.e., where $s(x)$ is measured) results in the full weight matrix \mathbf{W} used in equation (5).

2 Calibration method

To obtain the absolute value of the electric field, a calibration measurement on a known field is performed. Chng [1] *et al.* found that the measured E-FISH signal is strongly influenced by the electric field profile due to the Gouy phase shift of the focused beam. Therefore, the conventional calibration method for E-FISH experiments using Laplacian fields can lead to large errors. Nakamura [2] *et al.* evaluated the dependence of the error on the Rayleigh length and the targeted field length when applying the conventional calibration method. To avoid these errors, the calibrated field should have a similar spatial profile as the targeted electric field.

In this work, we designed rod-to-rod and rod-to-cylinder electrodes for the calibration of E_y and E_x , respectively. Figure 1 shows the calculated fields of the two pairs of calibration electrodes simulated by COMSOL Multiphysics. The field profiles have similar size and shape as the streamer generated under the conditions used in this work. The calculated fields are then forward-transformed to become the “calculated E-FISH signals”.

We then measure the E-FISH signals of the calibration electrodes. To increase the signal intensity, the highest voltages for both configurations below the breakdown threshold are used, which are 1.5 kV and 2.5 kV for E_y and E_x , respectively. Because the measurement range is limited within ± 15 mm due to the size of the window on the vessel, the measured signals are much shorter than the simulated ones and do not reach 0 at the boundary. The calibration constant C_{cal} is obtained by comparing the calculated and the measured E-FISH signals on a range of r over which both signals are reliable. For E_y this is $r = 2 - 6$ mm and for E_x this is $r = 5 - 10$ mm. This method shows robust results and little dependence on the exact parameters used.

3 Full processing method

In order to convert the measured intensities to electric field strengths, the following procedure is followed:

1. The intensities of the SH $I_{2\omega}$ and the fundamental beam I_ω are obtained by integrating the peak of the recorded traces over 4 ns. Then the measured signal per point is calculated as $s_{meas} = \sqrt{I_{2\omega}/I_\omega^2}$. To increase the signal-to-noise ratio, 40 measurements are averaged.
2. The background signal is subtracted using $s(x) = \sqrt{s_{meas}(x)^2 - s_{BG}^2}$, where $s_{meas}(x)$ is the measured signal as discussed above, and s_{BG} is the background signal, probably due to interference as discussed in section 4. The background is determined by a separate measurement without field, or, for E_x using the area below the streamer where there is no field expected. In this case the background is a function of the x coordinate.
3. The $s(x)$ data is made symmetric by flipping one side (in the x direction, around the symmetry axis) and averaging it with the other side.
4. The backwards inversion discussed in section 1 is used to convert the signal. The entire domain up to $r = 150$ mm (edge of the vessel) is used in this inversion. The solution is forced to be fully positive.
5. The solution is multiplied with C_{cal} as discussed in section 2 and converted to Townsend using the temperature and pressure.

4 Interference with other signals.

Second harmonic (SH) generation can happen through E-FISH, but also through asymmetries in solid materials. The latter is intentionally done in doubling crystals, which are used in lasers. In E-FISH measurements, generally lenses, mirrors, prisms and other optics are used as part of the setup. These components can generate unwanted SH radiation which is colinear and coherent with the E-FISH signal. In most works, this background signal is minimized by lowering the power of the input beam. The left-over background signal is then subtracted from the E-FISH measurements. However, the background SH can interfere with the E-FISH signal, which results in the following relation:

$$I = I_E + I_B + 2\sqrt{I_E I_B} \cos \phi, \quad (19)$$

with I the total intensity measured by the SH detector, I_B the background SH intensity, I_E the E-FISH signal and ϕ the phase difference between the background SH and E-FISH signal. The latter is proportional to the distance between the E-FISH measurement area and the SH-generating optics and to the wavevector mismatch (and thereby the gas type and density).

$\cos \phi$ switches sign for changing electric field polarity, which results in

$$\begin{aligned} I_+ &= I_E + I_B + 2\sqrt{I_E I_B} \cos \phi, \\ I_- &= I_E + I_B - 2\sqrt{I_E I_B} \cos \phi, \end{aligned} \quad (20)$$

where the two different components result from opposite field directions in the E-FISH measurement area (and thereby opposite phase at the point of interference).

Due to the asymmetry in equation (20), measured signals can be higher or lower than the real E-FISH signals. Simply subtracting the background (I_B) could therefore lead to negative measured intensities, which is clearly nonphysical. Also, when measuring electric fields which have two different polarities, which are expected to be symmetric either in space or time, this can lead to asymmetric measurement results.

Examples of this are phase-resolved measurements of (Laplacian) electric fields generated by applying a sinusoidal voltage to symmetric electrodes, leading to an asymmetry between the measured fields during the two half-waves. This has been observed and discussed by [3]. In our experiments, the electric field in the x -direction is expected to be symmetric around the streamer propagation axis due to the cylindrical symmetry. There, the field direction is reversed between the left and right halves. The asymmetry in these measurements can be seen in figure 2.

The error in the results can be much higher than the background signal itself due to the $2\sqrt{I_E I_B}$ term; this is illustrated in figure 3.

For measurements which do not have symmetric dual polarity signals, it is very difficult to determine if $\cos \phi$ is close to zero, which would allow a simple background subtraction.

There are a few ways to deal with the issue discussed above:

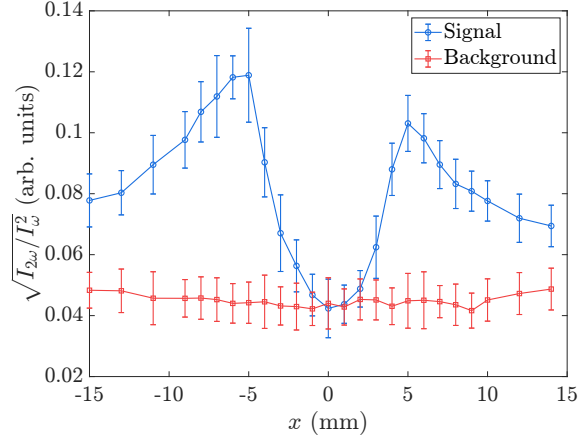


Figure 2: An example of asymmetric E_x measurement on a propagating single-channel streamer and the corresponding background signals.

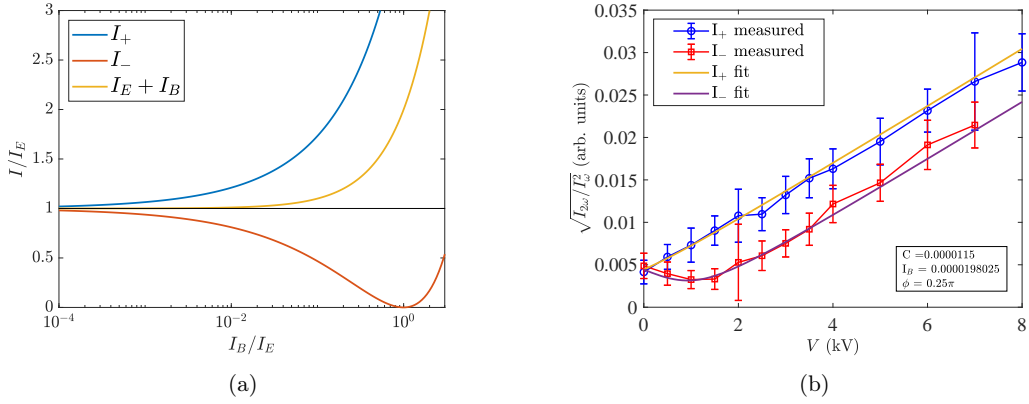


Figure 3: (a) Calculated ratio between the expected SH intensities for both field polarities (I_+ and I_-) and the E-FISH intensity, or the naively expected intensity ($I_E + I_B$) and the E-FISH signal as function of relative background level for $\cos \phi = 1$. (b) Measured E-FISH signal between symmetric electrodes with field in the x -direction under opposite polarities. Includes a fit of the calibration constant, the background intensity and $\cos \phi$.

1. Change the distance between E-FISH measurement area and SH-producing optics such that $\cos \phi \approx 0$ and a simple background subtraction is allowed. However, changes in ambient air pressure can already lead to deviations from this ideal case. For example, the horizontal distance between the discharge gap and the prism is about 1 m in our setup. A change of 20 mbar in air pressure changes $\cos \phi$ to 0.3.
2. For purely anti-symmetric cases (like E_x in our experiments), averaging both polarities (sides) suffices because in this case the last term in equations (20) drops out.
3. Minimizing the production of SH by windows and optics by lowering beam intensity and carefully choosing and cleaning the optics. One way to do it is using cross-beam E-FISH [4], where no beam separation optics is required.

If none of these are (or can be) applied, the background SH signal can lead to large errors in the measured E-FISH signals and thereby in the determined electric fields.

References

- [1] Tat Loon Chng, Svetlana M Starikovskaia, and Marie-Claire Schanne-Klein. Electric field measurements in plasmas: how focusing strongly distorts the e-FISH signal. Plasma Sources Science and

Technology, 29(12):125002, 2020.

- [2] Shin Nakamura, Masahiro Sato, Takashi Fujii, and Akiko Kumada. Optimization of beam shaping and error quantification of calibration approach using e-fishg based electric field measurements. Plasma Sources Science and Technology, 31(11):115020, November 2022.
- [3] Martina Mrkvičková, Lucia Kuthanová, Petr Bílek, Adam Obrusník, Zdeněk Navrátil, Pavel Dvořák, Igor Adamovich, Milan Šimek, and Tomáš Hoder. Electric field in aptd in nitrogen determined by efish, fns/sps ratio, alpha-fitting and electrical equivalent circuit model. Plasma Sources Science and Technology, 32(6):065009, June 2023.
- [4] S Raskar, K Orr, I V Adamovich, T L Chng, and S M Starikovskaia. Spatially enhanced electric field induced second harmonic (seefish) generation for measurements of electric field distributions in high-pressure plasmas. Plasma Sources Science and Technology, 31(8):085002, August 2022.